PROTEINS: Structure, Function, and Bioinformatics 58:407–417 (2005)

Receptor Rigidity and Ligand Mobility in Trypsin–Ligand Complexes

Olgun Guvench, Daniel J. Price, and Charles L. Brooks III*
Department of Molecular Biology (TPC-6), The Scripps Research Institute, La Jolla, California

ABSTRACT **The trypsin-like serine proteases comprise a structurally similar family of proteins with a wide diversity of biological functions. Members of this family play roles in digestion, hemostasis, immune responses, and cancer metastasis. Bovine trypsin is an archetypical member of this family that has been extensively characterized both functionally and structurally, and that preferentially hydrolyzes Arg/Lys–Xaa peptide bonds. We have used molecular dynamics (MD) simulations to study bovine trypsin complexed with the two noncovalent small-molecule ligands, benzamidine and tranylcypromine, that have the same hydrogen-bond donating moieties as Arg and Lys side-chains, respectively. Multiple (10) simulations ranging from 1 ns to 2.2 ns, with explicit water molecules and periodic boundary conditions, were performed. The simulations reveal that the trypsin binding pocket residues are relatively rigid regardless of whether there is no ligand, a high-affinity ligand (benzamidine), or a low-affinity ligand (tranylcypromine). The thermal average of the conformations sampled by benzamidine bound to trypsin is planar and consistent with the planar internal geometry of the benzamidine crystallographic model coordinates. However, the most probable bound benzamidine conformations are ±25° out of plane, implying that the observed X-ray electron density represents an average of densities from two mirror symmetric, nonplanar conformations. Solvated benzamidine has free energy minima at ±45°, and the induction of a more planar geometry upon binding is associated with ~1 kcal/mol of intramolecular strain. Tranylcypromine's hydrogen-bonding pattern in the MD differs substantially from that inferred from the X-ray electron density. Early in simulations of this system, tranylcypromine adopts an alternative binding conformation, changing from the crystallographic conformation, with a direct hydrogen bond between its amino moiety and the backbone oxygen of Gly219, to one having a bridging water molecule. This result is consistently seen with the CHARMM22, Amber, or OPLS-AA force fields. The trypsin–tranylcypromine hydrogen-bonding pattern observed in the simulations also occurs as the crystallographic binding mode of the Lys15 side-chain of bovine pancreatic trypsin inhibitor bound to trypsin. In this latter cocrystal, a bridging crystallographic water does reside between the side-chain's amino group and the trypsin Gly219 backbone oxygen. Furthermore, the trypsin–tranylcypromine simulations sample two different stable noncrystallographic binding poses. These data suggest that some of the electron density ascribed to tranylcypromine in the X-ray model is rather due to a bound water molecule, and that multiple tranylcypromine binding conformations (crystallographic disorder) may be the cause of ambiguous electron density. The combined trypsin–benzamidine and trypsin– tranylcypromine results highlight the ability of simulations to augment protein–ligand complex structural data by deconvoluting the effects of thermal and structural averaging, and by finding energetically optimal ligand and bound water positions for weakly bound ligands. Proteins 2005;58:407–417.** © 2004 Wiley-Liss, Inc.

Key words: benzamidine; tranylcypromine; protein–ligand; molecular dynamics

INTRODUCTION

The trypsin-like serine proteases comprise a structurally similar family of proteins with a wide diversity of biological functions. Members of this family include digestive enzymes[1,2]; leukocyte proteins that promote inflammation and mucous secretion,[3] and play roles in controlling infection[4,5] and in causing pulmonary[6] and hepatic disease[7]; complement proteins[8–11] that provide innate humoral immunity; hemostatic proteins[12]; tryptases, which play roles in asthma[13] and in influenza infection[14]; neuropsin, which may be involved in neural plasticity[15]; neurosin, which degrades α-synuclein, whose aggregation is seen in synucleinopathies such as Parkinson's disease[16]; prostate-specific antigen, which is clinically useful as a diagnostic for prostate cancer[17]; and urokinase-type plasminogen activator and plasminogen, which degrade extracellular matrix and facilitate cancer metastasis.[18] These proteins are all able to perform the identical catalytic

The Supplementary Materials referred to in this article can be found at http://www.interscience.wiley.com/jpages/0887-3585/suppmat/index.html

Grant sponsor: Fletcher Jones Foundation (fellowship support to O. Guvench). Grant sponsor: ARCS Foundation. Grant sponsor: NIH; Grant numbers: GM37554 and F32 AI49673.

*Correspondence to: Charles L. Brooks, Department of Molecular Biology (TPC-6), The Scripps Research Institute, 10550 N. Torrey Pines Road, La Jolla, CA 92037. E-mail: brooks@scripps.edu

Received 20 April 2004; Accepted 27 July 2004

Published online 1 December 2004 in Wiley InterScience (www.interscience.wiley.com). DOI: 10.1002/prot.20326

chemistry of hydrolyzing peptide bonds. The mechanism employs nucleophilic attack of a peptide bond by a serine side-chain that is part of a "catalytic triad" of residues comprised of serine, histidine, and aspartic acid, whose side-chains form a hydrogen-bond network.[19]

The biological activities of trypsin-like serine proteases are, in most cases, a product of their enzymatic activity.[20] Proteins that are hydrolyzed by the trypsin-like serine proteases include those that are converted into peptides during digestion, proproteins that are converted to active forms,[21] and G protein–coupled protease-activated receptors whose cleavage reveals covalently attached peptide agonists.[13,22] Part of the wide range of biology carried out by this family of enzymes is due to differential localization. For example, the hemostatic protein thrombin is found in the blood, while the digestive enzyme chymotrypsin is secreted into the digestive tract. The trypsin-like serine proteases' varying hydrolytic specificities for particular protein–peptide substrates are another reason for their functional heterogeneity, as can be seen in the examples of trypsin, chymotrypsin, and elastase. While these three enzymes all catalyze peptide bond hydrolysis, trypsin preferentially hydrolyzes peptide bonds immediately after positively charged side-chains, chymotrypsin after bulky aromatic side-chains, and elastase after small neutral side-chains.[23]

Bovine trypsin is an archetypical member of the trypsin-like serine proteases. It has been extensively characterized, both functionally and structurally [160 structures containing bovine trypsin or its proenzyme form trypsinogen were listed in the Structural Classification of Proteins (SCOP) database[24] as of 7/2004]. Among the crystal structures of bovine trypsin (subsequently referred to herein as "trypsin") are two complexes with the small-molecule ligands, benzamidine and tranylcypromine. Both benzamidine and tranylcypromine contain a single phenyl ring, and both have a net +1 charge at neutral pH [Fig. 1(a)]. Trypsin's specificity for cleaving Lys–Xaa or Arg–Xaa peptide bonds is reflected in these ligands' structures: The +1 net charge of benzamidine is due to an amidine functional group, similar to the guanidinium moiety of Arg side-chain, and the +1 net charge of tranylcypromine is due to an amino group, like that on Lys side-chain. Per the cocrystal structures of these ligands with trypsin,[28,29] their binding modes are nearly identical [Fig. 1(b)]. Both ligands in their respective crystal structures form direct hydrogen bonds to the Asp189 side-chain and to the Gly219 backbone oxygen (chymotrypsin numbering of Hartley and Kauffman[30]). Despite these structural similarities, benzamidine and tranylcypromine have substantially different binding affinities. Benzamidine binds quite strongly with a K_i of 0.018 mM[31] in contrast to tranylcypromine, whose K_i is 13 mM[29] ($\Delta\Delta G$ = 4 kcal/mol).

With the aim of furthering understanding of bound ligand mobility, water structure in the binding site, and the effects of ligand binding on trypsin conformational flexibility, we have used molecular dynamics (MD) simulations to study bovine trypsin and its complexes with benzamidine and tranylcypromine. The simulations utilize explicit solvent with periodic boundary conditions and include all protein, ligand, and solvent degrees of freedom. Analysis of the data shows that trypsin's binding site is rigid, and that this rigidity is ligand independent. Benzamidine acquires intramolecular strain with binding, but nonetheless does retain some internal mobility. The MD data suggest two noncrystallographic binding modes for tranylcypromine, along with an additional bound water position. These latter findings are discussed in the context of a trypsin–bovine pancreatic trypsin inhibitor cocrystal whose structure supports the simulation results.

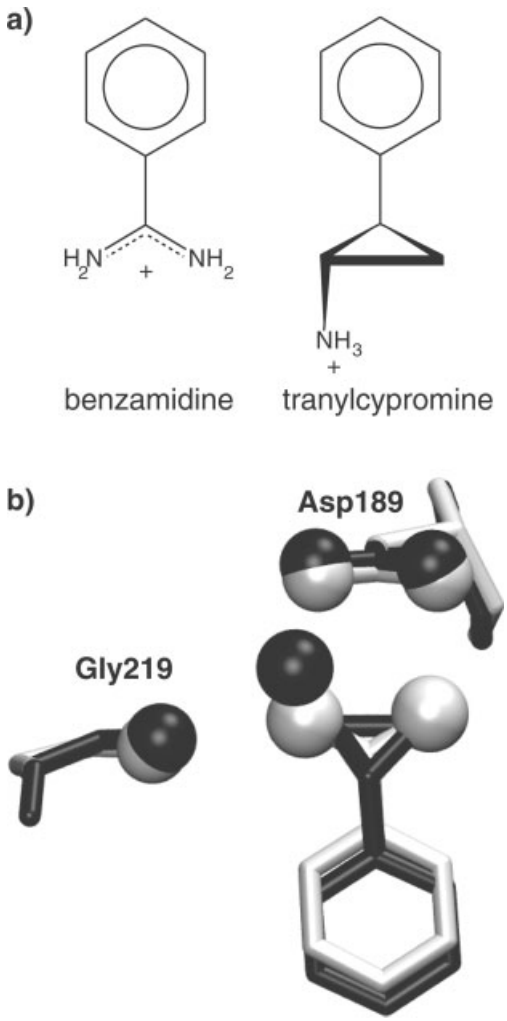

Fig. 1. Benzamidine and tranylcypromine. (**a**) Chemical structures. Chemtool[25] is used to create this and all other 2D representations. (**b**) Crystallographic binding modes. The cocrystal structures of benzamidine and tranylcypromine with trypsin (PDB IDs: 3ptb and 1tnl, respectively) are least-squares aligned using the trypsin C_α atoms. Heavy-atoms for the two ligands and for Asp189 and Gly219 are shown. Spheres correspond to ligand nitrogen atoms, Asp189 side-chain oxygens, and the backbone oxygen of Gly219. The benzamidine cocrystal is in white, and the tranylcypromine cocrystal is in black. VMD[26] and Tachyon[27] were used to create this and all other 3D representations.

MATERIALS AND METHODS

The trypsin–benzamidine and trypsin–tranylcypromine X-ray crystal structures[28,29] [Protein Data Bank (PDB)

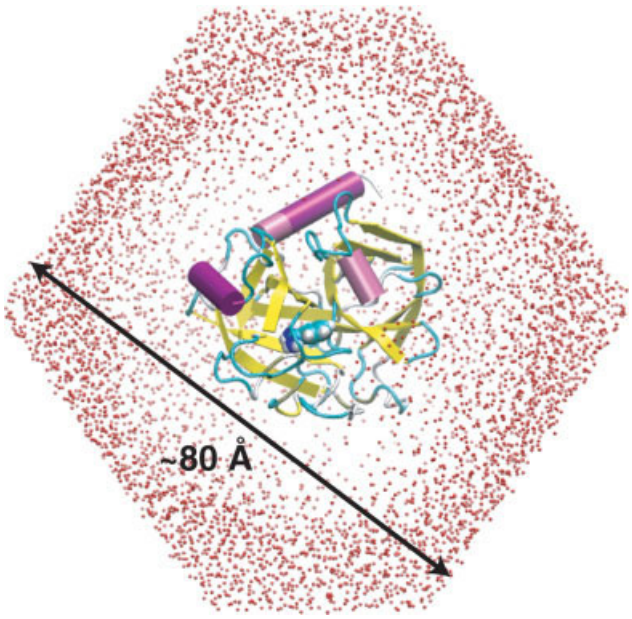

Fig. 2. Solvated trypsin–benzamidine system.

IDs: 3ptb and 1tnl, respectively] serve as the starting point for the MD simulations. Simulations are done with the CHARMM molecular mechanics program[32] and the CHARMM22 force field,[33] and use the TIP3P water model[34] modified for the CHARMM force field. Benzamidine and tranylcypromine atom types and the associated Lennard–Jones nonbonded parameters are assigned based on CHARMM22 atom-type definitions, and partial charges are taken from the Ligand–Protein Database[35] (Supplementary Material). Adiabatic quantum mechanical energy profiles for rotation about the bonds to the phenyl moieties of benzamidine and tranylcypromine are calculated at the HF/6-31G*//HF/6-31G* level using Spartan.[36] The corresponding benzamidine torsion is empirically fit to reproduce the quantum mechanical data, the tranylcypromine torsion is fit to the quantum mechanical data using the least-squares method with singular value decomposition,[37] and other missing ligand bonded parameters are based on the minimum energy geometries from the Hartree–Fock calculations and similarity to CHARMM22 bonded parameters (parameters are available from the authors upon request).

Missing trypsin–benzamidine cocrystal structure atoms are placed using force field equilibrium geometries. Based on inspection of adjacent residues, His40 and His91 are protonated at the ϵ position, and His57 is protonated at the δ position. All crystallographic waters are retained, and additional water molecules are added so as to create a truncated octahedron, with a minimum of a 14-Å water layer between the octahedron edges and the nearest solute atoms. The complete solvated system consists of 38,969 atoms: 3220 protein atoms, 18 benzamidine atoms, 1 Ca^{2+} cation, and 35,730 water atoms (Fig. 2). The solvated trypsin–tranylcypromine system is created by first deleting benzamidine from the trypsin–benzamidine system, followed by adding tranylcypromine coordinates from the trypsin–tranylcypromine cocrystal structure after least-squares alignment of the trypsin molecules' C_α atoms. The system consisting of trypsin without a ligand is created by deleting benzamidine from the trypsin–benzamidine system. Thus, apart from the ligands, all three systems have the same number of particles and initial coordinates.

Periodic boundary conditions are used,[38] and the SHAKE algorithm[39] is employed to constrain bonds to hydrogen atoms to their equilibrium values and keep the water geometry rigid. Electrostatic interactions are smoothly truncated to 0 kcal/mol at 12 Å using atom-based force shifting, and Lennard–Jones interactions are smoothly switched to 0 kcal/mol at 12 Å using a sigmoidal function between 10 Å and 12 Å.[40] Since it was not known a priori whether the nonbonded energy terms alone were sufficient to maintain coordination geometry on the nanosecond time scale, the structural Ca^{2+}, located a distant 20 Å from the binding pocket, was kept near its crystallographic position using restraints to adjacent protein atoms. Harmonic restraints with force constants of 10*(particle mass) kcal*mol^{-1}*Å^{-2}*amu^{-1} are applied to all protein heavy-atom positions, and the systems are energy minimized with 100 steps of the steepest descent algorithm.[41] They are then equilibrated with 20-ps of MD simulation at a temperature of 298 K, 1 atm of pressure, and with harmonic restraints on protein backbone heavy-atom positions using force constants of 5*(particle mass) kcal*mol^{-1}*Å^{-2}*amu^{-1}. This is followed by another 80 ps of equilibration employing unrestrained MD simulation at the same temperature and pressure. A timestep of 2 fs is used for integration of the equations of motion with the leapfrog version of the Verlet integrator,[42] constant temperature is maintained by reassigning velocities, if the average kinetic temperature of the system over 200 dynamics steps drifts ±5 K from the target temperature, and constant pressure is achieved by a Langevin piston,[43] with a mass of 10 amu and a collision frequency of 100 ps^{-1}. All subsequent MD simulations are performed at 298 K using the above thermostat method and at constant volume. The constant volume systems have as dimensions the final dimensions of the truncated octahedra at the end of the 100-ps constant pressure equilibration trajectories. The minimum dimension of a truncated octahedron is the distance from the centroid of one hexagonal face to the centroid of the opposite hexagonal face; this minimum dimension is 79.4387 Å, 79.3821 Å, and 79.2602 Å, respectively, for the trypsin–benzamidine, trypsin–tranylcypromine, and unliganded trypsin constant volume simulations. Three 1-ns MD production simulations are performed on both of the trypsin–ligand systems, starting from the final snapshots from the respective equilibration MD trajectories but with different random initial velocities so as to generate different trajectories. A single 1-ns control production simulation is performed on the unliganded trypsin system. Snapshots for subsequent analysis are taken every 100 dynamics steps during the production phase of the simulations.

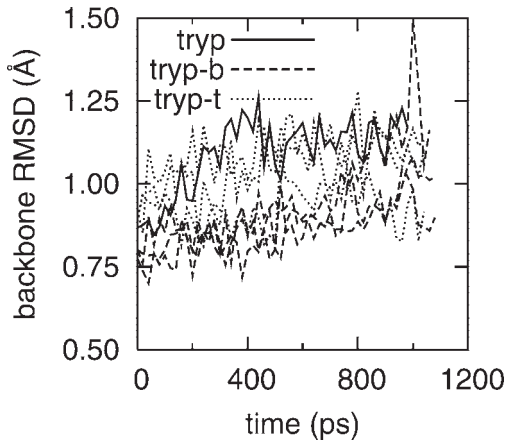

Fig. 3. Trypsin backbone RMSD relative to X-ray crystal structure: tryp = 1 MD trajectory of unliganded trypsin; tryp-b = 3 MD trajectories of trypsin–benzamidine; tryp-t = 3 MD trajectories of trypsin–tranylcypromine. All MD snapshots are least-squares aligned with the backbone atoms of the 3ptb trypsin X-ray crystal structure coordinates. Data from every 10,000th MD step (20 ps) are shown.

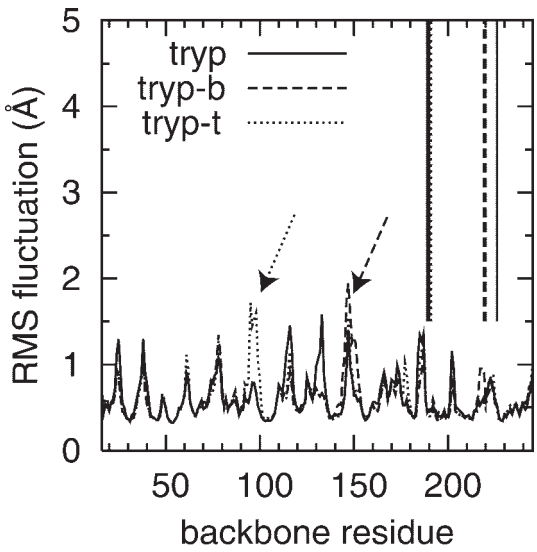

Fig. 4. Trypsin residues' backbone atom RMS fluctuations in MD simulations: tryp = unliganded trypsin; tryp-b = trypsin–benzamidine; tryp-t = trypsin–tranylcypromine. For tryp-b and tryp-t, data from three 1-ns production trajectories are combined. Solid vertical lines indicate trypsin residues within 3 Å of both benzamidine and tranylcypromine in their respective MD average structures. Dashed vertical lines indicate residues within 3 Å of benzamidine in the MD average structure. Dotted vertical lines indicate residues within 3 Å of tranylcypromine in the MD average structure.

RESULTS AND DISCUSSION

Trypsin

Trypsin experiences little drift from the X-ray crystallographic coordinates during the seven 1-ns production phase MD simulations. The 3 trypsin–benzamidine, 3 trypsin–tranylcypromine, and 1 unliganded trypsin trajectories all maintain backbone root-mean-square deviation (RMSD) values in the range of 0.75–1.25 Å relative to the X-ray crystal structure coordinates (Fig. 3). Three of the 7 trajectories' RMSD values have plateaued by 500 ps and a fourth's by 800 ps, and thereafter fluctuate between 1.0 Å and 1.25 Å. A fifth samples RMSD values > 1.0 Å in the 500- to 800-ps interval and returns to a value < 1.0 Å by its end. A fluctuation to 1.50 Å backbone RMSD is seen near the end of one of the trypsin–benzamidine trajectories. The fluctuation is transient, and the trypsin structure returns to a backbone RMSD of 1.09 Å within 80 ps. The close similarity to the X-ray structure maintained by all 7 simulations is indicative of a rigid, stable protein structure, in agreement with previous experimental and simulation work.[28,29,44–51]

Trypsin's rigidity is confirmed in greater detail in a residue-by-residue analysis of the nanosecond time scale positional fluctuations. Figure 4 shows the root-mean-square (RMS) fluctuations about the average atomic positions of the backbone atoms averaged over each residue. The average positions of trypsin backbone atoms are calculated from the MD snapshots after least-squares alignment with the trypsin–benzamidine cocrystal structure backbone atoms. The fluctuations are small, and there is no difference in the fluctuations seen in the unliganded trypsin, trypsin–benzamidine, and trypsin–tranylcypromine systems except for the two cases denoted by the arrows.

The peak at the dashed arrow is due to motion at the tip of a solvent-exposed loop toward the end of one of the 3 trypsin– benzamidine simulations, and is the same motion as that which registers as the previously mentioned fluctuation to 1.50 Å backbone RMSD. The largest fluctuation value in this peak corresponds to Ser147, whose B-factors are 26 Å^2 in the trypsin–benzamidine cocrystal and range from 45 Å^2 to 49 Å^2 in the trypsin–tranylcypromine cocrystal, and which is located a distant 13 Å from the ligand binding site. Large B-factors such as these can be indicative of thermal motion in individual molecules, averaging of data across conformationally heterogeneous molecules in the crystal ("disorder"), or a combination of these.[52] The residues Gly142 through Pro152 are one of 3 loop regions in the trypsin "activation domain." In the proenzyme trypsinogen, these activation domain loops are disordered.[53–55] After cleavage of the N-terminal hexapeptide of trypsinogen to form trypsin, the new N-terminus residue Ile16 is able to bind to a pocket formed by the activation domain loops, which become ordered.[56] The observed fluctuation may represent residual mobility in the Gly142 through Pro152 loop.

The peak at the dotted arrows is due to a minor conformational change in a solvent-exposed loop that is most prominent in 1 of the 3 trypsin–tranylcypromine simulations. The largest value in this peak is from Thr98, which is located at the tip of this loop, 14 Å from the ligand binding site, and whose B-factors are 10 Å^2 in the trypsin–benzamidine cocrystal and range from 15 Å^2 to 17 Å^2 in the trypsin–tranylcypromine cocrystal. These B-factors are not particularly large; therefore, this region is well ordered and static in the crystalline form. A possible contributor to this crystallographic structural stability is a hydrogen-bonded crystal contact between the loop's Asn97 backbone oxygen and the side-chain of Lys159 of an adjacent trypsin

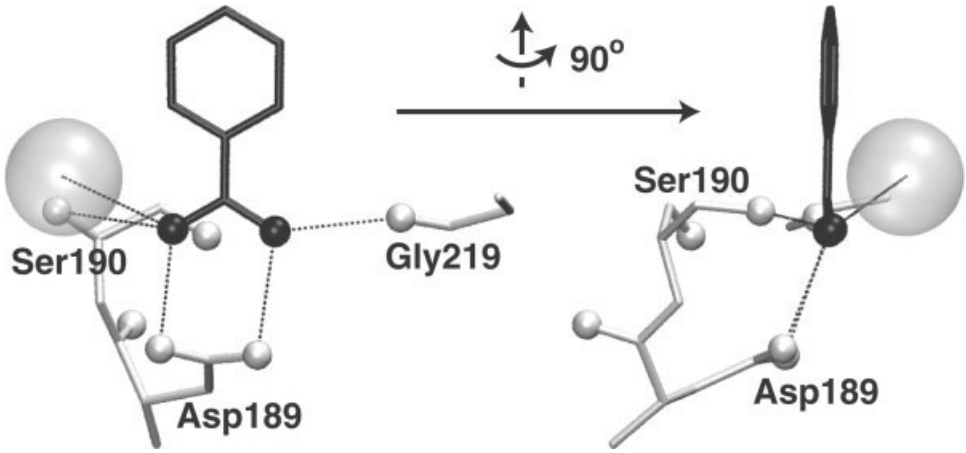

Fig. 5. Benzamidine hydrogen-bonding to trypsin. Coordinates are from 3ptb. Heavy-atoms for benzamidine (black), and Asp189, Ser190, and Gly219 (white) are shown. Small solid spheres correspond to benzamidine nitrogen atoms and trypsin oxygen atoms. The large transparent sphere is a crystallographic water. Thin dotted lines represent hydrogen bonds.

molecule in both the cocrystal structures. The absence of this crystal contact would be expected to decrease the structural stability of the loop, and the observed fluctuation in the simulation data likely reflects this.

In contrast to the 2 solvent-exposed loops' mobility, residues within 3 Å of the ligands, denoted by vertical lines in Figure 4, show little mobility. These proximal residues' fluctuations are also independent of the binding affinity of the ligands, or even their presence. The binding pocket's observed rigidity is in line with crystal structures of unliganded trypsin (2ptn[57]), trypsin–benzamidine (3ptb[28]), and trypsin–tranylcypromine (1tnl[29]) wherein these residues are neatly superimposed after least-squares alignment of the proteins' backbone atoms. The same trend in fluctuations is evident in the side-chain atoms (data not shown).

Benzamidine

Benzamidine's amidine group is chemically similar to the guanidinium moiety of the Arg side-chain. This chemical similarity is reflected in the identical hydrogen-bonding pattern to trypsin exhibited by benzamidine and the Arg15 side-chains of protein inhibitors of trypsin (4tpi,[58] 1ejm,[59] and 1f2s[60]). Hydrogen bonding involves the backbone oxygen of Gly219, both side-chain oxygens of Asp189, the Ser190 side-chain oxygen, and a crystallographic water (Fig. 5). As anticipated from its high binding affinity, benzamidine maintains this hydrogen-bonding pattern throughout the three 1-ns production simulations. Additionally, the crystallographic water molecule hydrogen-bonded to benzamidine is not exchanged for another water molecule during any of the 3 MD simulations.

Benzamidine has a single internal rotational degree of freedom about the bond connecting its amidine and phenyl moieties. The 0 K quantum mechanical potential energy profile for rotation of this dihedral χ (crystallographic naming: C2–C1–C7–N1) calculated while developing molecular mechanics parameters for benzamidine showed a minimum at +45° (and identically at −45°, +135°, and −135° due to symmetry), in contrast to the X-ray crystal structure value of −2.1°. A 2-ns MD simulation of solvated benzamidine revealed that the quantum mechanical minima were retained in bulk water at 298 K using the molecular mechanics model, as χ values of ±45° and ±135° were sampled with the highest probabilities. In contrast, when bound to trypsin, the conformations sampled with the highest probabilities had χ values of ±25° [Fig. 6(a)]. Based on the torsional energetic profile, this decrease in χ upon binding represents approximately +1 kcal/mol of strain. The geometries of benzamidine with χ values of 0°, 25°, and 45°, which correspond to crystallographic, MD bound most probable, and MD unbound most probable conformations, are substantially different [Fig. 6(b)].

The MD simulations did not include effects on the electronic structure of benzamidine due to the presence or absence of trypsin, since a molecular mechanics force field was employed and the benzamidine parameters were identical for bound and unbound trajectories. Despite this, the Coulomb and Lennard–Jones fields in the trypsin binding pocket force the bound benzamidine to be 20° closer to planar than when unbound. It is possible that electronic effects cause a further change in the free energy profile for rotation about χ and lead to a minimum at or close to 0°, in line with the X-ray coordinates. However, a free energy minimum at $\chi = 0°$ for benzamidine bound to trypsin is not required to produce a crystallographically determined electron density that is best fit by nearly planar benzamidine coordinates. With two nonplanar free energy minimum conformations related by mirror symmetry (e.g., $\chi = \pm 25°$), rapid thermal interconversion between conformations and/or spatial averaging across complexes in the crystal containing one or the other conformation would lead to planar electron density. Using the combined χ data from the three 1-ns trypsin–benzamidine MD simulations [Fig. 6(a)], the average value of χ is +1.7°, in close agreement with the crystallographic coordinates. Furthermore, atomic displacements caused by $\chi = \pm 25°$ relative to $\chi = 0°$ are on the order of 1 Å;

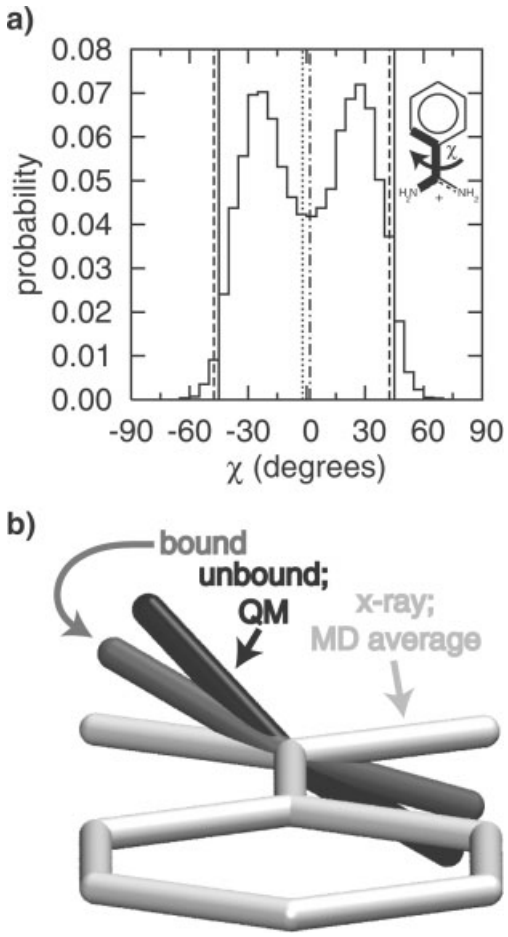

Fig. 6. X-ray crystallographic and MD conformations of benzamidine. (**a**) χ torsion angle (atoms C2–C1–C7–N1 of benzamidine in the 3ptb trypsin–benzamidine X-ray cocrystal structure) probability histogram from MD data. Data are combined from three 1-ns simulations of benzamidine complexed with trypsin and are binned in 5° increments. Solid vertical lines correspond to the Hartree–Fock minimum energy conformations; dashed vertical lines correspond to the most probable χ values from a single 2-ns MD simulation of solvated benzamidine; the dotted line corresponds to the χ value of benzamidine in the trypsin–benzamidine cocrystal structure; and the dotted dashed line corresponds to the average χ value determined from the histogram data. For benzamidine complexed with trypsin, the X-ray crystal structure value of χ is $-2.1°$, the MD average value of χ is $+1.7°$, and the MD most probable values of χ are the bins $+25°$ to $+30°$ and $-25°$ to $-20°$. (**b**) χ torsion angle: $\chi = 0.0°$ (white), $+25°$ (gray), and $+45°$ (black).

therefore, B-factors for this density would be expected not to be large, and indeed they are not (19.86 Å^2).[28] The current results show that molecular mechanics parameterization using the 0 K quantum mechanical potential energy surface for rotation about χ yields results consistent with the X-ray data, though the gas-phase quantum mechanical and solvated unbound molecular mechanical data have minima at $\pm45°$ and $\pm135°$, not at 0° and 180°.[50]

In addition to decreasing the most probable value of χ from $\pm45°$ when unbound to $\pm25°$ when bound, the trypsin environment also prevents sampling of the conformationally equivalent values of $\pm155°$. In none of the three 1-ns trypsin–benzamidine trajectories does benzamidine sample χ values other than those near $\pm25°$; that is, no ring flips are seen. In contrast, multiple ring flip events occur in the single 2-ns simulation of solvated benzamidine, and χ values about $\pm45°$ and $\pm135°$ are sampled. Quantitative conclusions cannot be drawn from this observation, but it is evident that trypsin increases the barrier for ring flipping.

Five other trypsin–benzamidine complexes were found in a search of the PDB: 1bty, 1tio, 2tio, 1ce5, 1j8a. The χ values for the equivalent benzamidine atoms in these 5 structures range from $-6.6°$ to $-18.0°$. The mean χ value for the set is $-11.5°$, with a standard deviation of 4.3°. Including 3ptb in the set decreases the mean to $-9.9°$ and increases the standard deviation to 5.4°. No correlation between the χ values and the resolution, benzamidine heavy-atom B-factors, temperature of data collection, or presence of an adjacent crystallographic phosphate molecule was found, and all structures were orthorhombic ($P2_12_12_1$). Though all the crystallographic values are closer to planar than the unbound trypsin free energy minima at $\pm45°$ and the bound free energy minima at $\pm25°$, they are all slightly negative. A simple estimate based on the observed χ frequency histogram and the scaling required to induce an asymmetry in probabilities consistent with an average value of $-9.9°$ suggests that the free energy difference between positive and negative χ values in the bound state is approximately the thermal energy RT at 298 K (0.6 kcal/mol).

Tranylcypromine

Tranylcypromine shares benzamidine's phenyl group but provides a hydrogen-bonding moiety in the form of an amino group instead of an amidine. The only PDB structure of trypsin–tranylcypromine (1tnl) includes hydrogen atom coordinates and shows direct hydrogen bonds from tranylcypromine's amino moiety to one of Asp189's side-chain oxygens and to Gly219's backbone oxygen [Fig. 1(b)]. These two residues satisfy the hydrogen-bonding potential of 2 of the 3 amino group protons. There are no hydrogen-bond acceptor atoms within 3.0 Å of the third proton, and of the 2 hydrogen-bond acceptors within 3.5 Å, 1 forms an N—H : O angle of 59.8° and the other an H : O—C angle of 86.3°, which rules out these as forming weak, long hydrogen bonds. It is also not possible that this proton hydrogen-bonds to disordered water whose electron density is not seen, since there is no room to insert a water molecule. Therefore, based on the crystallographic coordinates, this third tranylcypromine amino group proton is a buried unsatisfied hydrogen-bond donor.

During the first 20 ps of the MD equilibration phase, tranylcypromine undergoes a change in its orientation in the binding pocket. Most notably, the tranylcypromine amino group moves from being hydrogen-bonded to one of Asp189's side-chain oxygens to being hydrogen-bonded to the other. This change from the crystallographic binding pose also causes the loss of the amino group's hydrogen bond to Gly219. Crystallographic water 415 (HOH415) undergoes a 3.54 Å translation in this 20-ps timespan to move from its initial position to the position formerly occupied by the tranylcypromine amino group. In this new

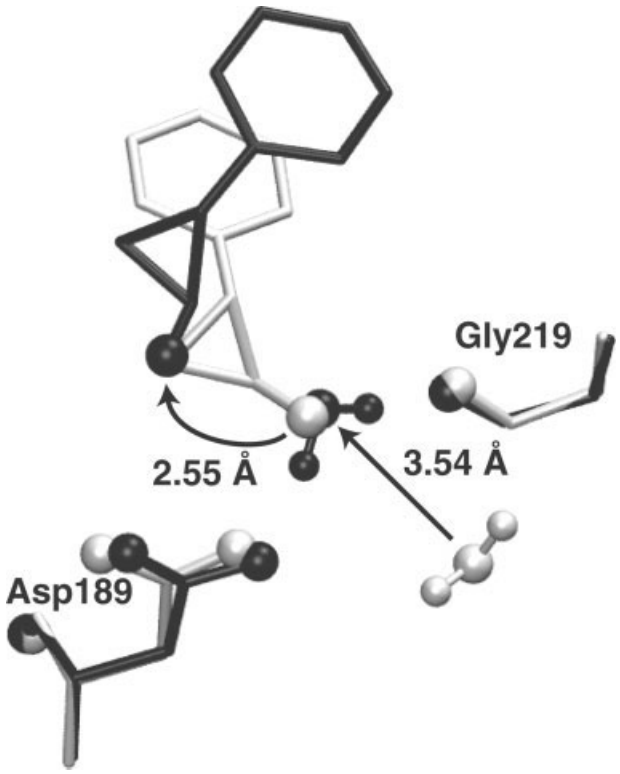

Fig. 7. Insertion of bridging water between tranylcypromine and Gly219 during MD equilibration: 0-ps (white) and 20-ps (black) conformations are shown. The crystallographic water molecule undergoes a 3.54 Å displacement to form a bridging hydrogen bond between tranylcypromine and Gly219, whose direct hydrogen bonding is lost due to a 2.55 Å displacement of the tranylcypromine amino group. Tranylcypromine nitrogen and trypsin oxygen atoms are shown as spheres. The snapshots have been least-squares aligned using all trypsin backbone atoms.

position, HOH415 acts as a hydrogen-bond acceptor to tranylcypromine and a hydrogen-bond donor to Gly219, thereby converting the crystallographic direct hydrogen bond between tranylcypromine and Gly219 to a bridged hydrogen bond (Fig. 7).

In its crystal pose, HOH415 serves as a hydrogen-bond donor to Ser217 O and Lys224 O, and a hydrogen-bond acceptor for Gln221 N. Ser217 compensates for loss of hydrogen bonding to HOH415 by orienting its carbonyl oxygen into the bulk solvent during the course of the 100 ps of equilibration. The Lys224 backbone oxygen is hydrogen-bonded to HOH562, as well as to HOH415 in the crystal structure. Lys224 backbone oxygen's hydrogen-bonding potential is satisfied despite the loss of a hydrogen bond to HOH415 during equilibration by maintaining a hydrogen bond to HOH562. Backbone alignment of the 0-ps and 100-ps conformations from the equilibration phase shows a 0.89 Å displacement of HOH562. This small displacement allows it to maintain a hydrogen bond with Lys224, while also forming a new hydrogen bond with the amide hydrogen of Gln221, which shows a 1.07-Å displacement. The formation of the Gln221 : HOH562 hydrogen bond compensates for the loss of a hydrogen bond between Gln221 and HOH415 due to HOH415's movement.

The conformational changes in tranylcypromine and HOH415, completed in the first 20 ps of the equilibration phase, occur while there are positional restraints on the protein backbone heavy atoms. These restraints keep sampled trypsin conformations very close to those in the crystal structure: The residues within 5 Å of HOH415 at 0 ps (Tyr172, Asp189, Gly216 to Gln221, Lys224, and Pro225) have an all-atom RMSD of 0.83 Å when comparing the 0-ps conformation with the 20-ps conformation. The significant tranylcypromine and HOH415 motion during this timespan shows that the crystallographic positions for tranylcypromine and HOH415 are not stable in the field generated by the crystallographic protein coordinates. Examination of crystal contacts shows that there are none involving the ligand, thereby ruling them out as a source of the difference between the simulation and crystallographic model ligand conformations.

To rule out the possibility of bias caused by creating the solvated trypsin–tranylcypromine system by using the protein and crystallographic water coordinates from 3ptb (see Materials and Methods section), a second solvated trypsin–tranylcypromine system was built directly using the trypsin, crystallographic water, and tranylcypromine coordinates from 1tnl and rerun with the same equilibration protocol. The heavy-atom RMSD for the trypsin coordinates of 3ptb and 1tnl is 0.78 Å, and 1tnl's crystallographic water molecules 269 and 395 are located at the same positions as 3ptb's 415 and 562, respectively; thus, the starting conformation of the second system was very similar to the first, and no structural artifacts in the first were apparent upon visual inspection (subsequent references to 1tnl water numbers will be immediately followed by the 3ptb numbering in brackets for clarity). The snapshot at 20 ps of equilibration showed identical changes in the positions of tranylcypromine and HOH269 [415] compared to the previous simulation, that is, tranylcypromine amino group motion away from Gly219, leading to loss of the direct hydrogen bond and insertion of HOH269 [415] to form a bridging hydrogen bond. These changes in tranylcypromine and water structure were maintained to the end of the 100-ps equilibration.

To rule out force field bias, we reran the equilibration protocol (as detailed in the Materials and Methods section) on the system constructed directly from the 1tnl coordinates using the Amber[61] and OPLS-AA[62,63] force fields as implemented in the CHARMM simulation package. Tranylcypromine parameters appropriate for Amber were assigned using Antechamber,[64] with partial charges averaged to obtain identical charges on chemically equivalent atoms, OPLS-AA tranylcypromine parameters were obtained from the OPLS-AA database, and dihedral parameters for rotation about the bond to the phenyl ring were fit for each force field, as described in the Materials and Methods section. Both the Amber and OPLS-AA simulations exhibited the same change in tranylcypromine amino group and HOH269 [415] positions by 20 ps of equilibration as in the simulations with the CHARMM22 force field, and once formed, this tranylcypromine : HOH269 [415] : Gly219 hydrogen-bond network persisted to the end of

these 100-ps equilibrations. This consistency of results regardless of the choice of force field is not unexpected given that current biomolecular force fields are similarly accurate.[65]

Finally, to test for the possibility that the protein was insufficiently restrained while relaxing the other degrees of freedom, we reran the equilibration protocol (1) with restraints on all trypsin heavy atoms and (2) with restraints on all trypsin and tranylcypromine heavy atoms. With restraints on all trypsin heavy atoms for the full 100 ps, the change in tranylcypromine conformation and the formation of the insertion of the bridging water is completed by 20 ps and maintained to 100 ps, while the all-atom RMSD for the 0-ps and 100-ps trypsin conformations is only 0.43 Å, providing further evidence that tranylcypromine and HOH269 [415] are not stable in the field generated by the crystallographic trypsin coordinates. With restraints on all trypsin and tranylcypromine heavy atoms during the first 20 ps, the direct hydrogen bond between tranylcypromine and Gly219 is predictably enforced. Nonetheless, HOH269 [415] moves 0.97 Å away from its 0-ps position and in the direction of the tranylcypromine amino group and Gly219 O, showing that it has a clear energetic preference for association with these moieties, though further motion is prevented by steric hindrance from the restrained degrees of freedom. Restraints are released at 20 ps, and by 100 ps the tranylcypromine : Gly219 direct hydrogen bond is lost, and is instead bridged by HOH269 [415], as also occurs in all the other equilibration trials.

Having ruled out bias due to starting conformation, use of a particular force field, and choice of restraints while relaxing the solvent as possible causes of the loss of direct hydrogen bonding between tranylcypromine and Gly219, and insertion of a bridging water molecule between them, we analyzed the production MD data to investigate whether this new geometry was a stable one. Of the three 1-ns production trajectories, 2 retain a tranylcypromine conformation for their full duration, very similar to that at the end of the equilibration phase, including the bridging water molecule. The third does so for the first 80 ps, after which the tranylcypromine amino group goes from having hydrogen bonds to HOH415 and one of the two Asp189 side-chain oxygens to having hydrogen bonds to both Asp189 side-chain oxygens. At 500 ps into this third trajectory, tranylcypromine undergoes a 180° rotation about its longest axis, and in this conformation, the steric bulk of the methylene group in the 3-membered ring prevents any approach of HOH415 to within hydrogen-bonding distance of the amino group. Despite these differences with the other two trajectories, this trajectory also maintains the HOH415 : Gly219 hydrogen bond for its duration in place of the crystallographic direct tranylcypromine : Gly219 hydrogen bond.

Figure 8 illustrates the sampled tranylcypromine conformations during production MD in the context of the tranylcypromine X-ray coordinates, as well as X-ray coordinates from a trypsin–bovine pancreatic trypsin inhibitor (BPTI) cocrystal (2ptc[28]). BPTI is a 58–amino acid protein inhibitor to trypsin, whose Lys15 side-chain occupies the same binding pocket as benzamidine and tranylcypromine. MD average structure **i** is from the combined data of two 1-ns trajectories, and is essentially the same as the conformation at the end of the equilibration phase (compare to black conformations in Fig. 7). MD average structure **ii** is from the final 500 ps of the third 1-ns trajectory. Apparent in Figure 8 is the similarity in the hydrogen-bond patterns of **i**, **ii**, and BPTI Lys15, and the difference between them and the tranylcypromine X-ray binding mode. In particular, the former 3 all lack a hydrogen bond to Gly219, while sharing very similar positioning of their amino groups in the binding site. Additionally, the bridging water molecule seen in the simulations (Fig. 7) occupies the same site as crystallographic water HOH414 in the trypsin–BPTI cocrystal (Fig. 8), in contrast to the trypsin–tranylcypromine cocrystal coordinates in which the ligand amino group occupies the electron density at this position. Finally, the preservation of the internal geometry of tranylcypromine in the 2 average structures implies that tranylcypromine samples 2 distinct binding modes, and not a broad continuum of probable conformations, for were the latter the case, there would be distortions in the internal geometries of the average structures. This is confirmed by the small values of the isotropic RMS fluctuations about the average coordinates of tranylcypro-

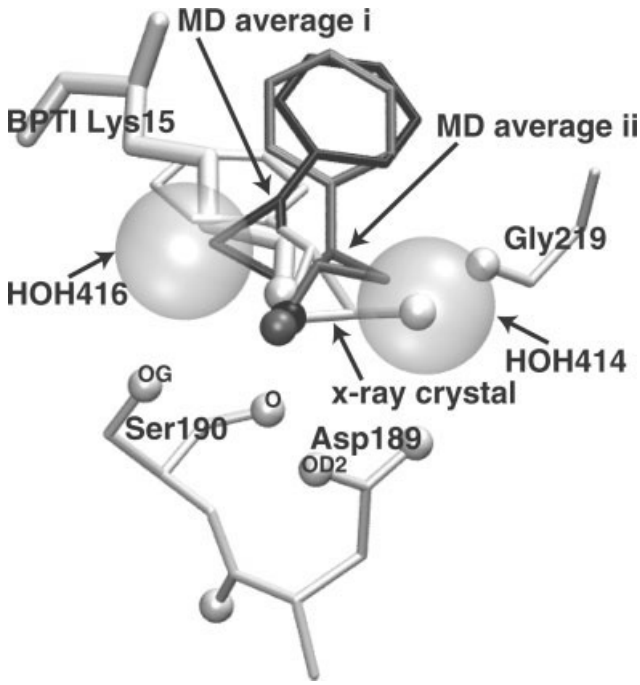

Fig. 8. X-ray crystallographic and average MD conformations of tranylcypromine, and the X-ray crystallographic conformation of BPTI Lys15, all complexed with trypsin. Structures are least-squares aligned using trypsin C_α atoms from the trypsin–BPTI cocrystal (2ptc). Tranylcypromine and BPTI Lys15 X-ray crystal structure coordinates are in white, and average coordinates from MD simulations are in black (**i**) and gray (**ii**). Also in white are trypsin Asp189, Ser190, Gly219, and the 2 crystallographic water sites proximal to BPTI Lys15, all from the trypsin–BPTI cocrystal. Tranylcypromine and BPTI Lys15 side-chain nitrogen atoms, and Asp189, Ser190, and Gly219 oxygen atoms are shown as small solid spheres; water sites are shown as large transparent spheres.

mine heavy atoms, which are in the ranges 0.44–0.82 Å for **i** and 0.43–1.07 Å for **ii**.

The simulations, along with the trypsin–BPTI cocrystal, suggest that the electron density attributed to the tranylcypromine amino group may rather be due to a bound water molecule. In the simulations, the replacement of the tranylcypromine amino group with a water molecule requires motion of a nearby crystallographic water, since bound tranylcypromine occludes access of bulk water to this position, and the time scale of the simulations precludes an unbinding–binding event that could allow for such access. An alternative to movement of a current crystallographic water is that of an additional bound water molecule placed at this position. To evaluate this possibility, we ran 3 additional MD trajectories of trypsin– tranylcypromine, each of length 1.2 ns. For the starting conformation of these three, we used the same starting conformation as previously but changed the coordinates of one of the bulk water molecules located at the edge of the truncated octahedron to those of the water molecule occupying the same site as HOH414 in the first of the average structures discussed above, and thereby increased the number of bound water molecules by one. After 2000 steps of minimization, the system was simulated in the NVT ensemble, using the same dimensions as for the previous 3 simulations, and as before different random velocities were assigned at 0 ps so as to obtain 3 different trajectories. Harmonic restraints on backbone heavy-atom positions were in effect during the 0-ps–20-ps interval, and were subsequently released. At 200 ps, the temperature window for velocity reassignment was decreased to ± 0.5 K to maintain tighter temperature control, and the simulations were continued another 1 ns. The previous 3 trajectories that did not include the extra water in the binding pocket were continued for another 1.2 ns each, and during the last 1 ns, the temperature window for these trajectories was also decreased to ± 0.5 K.

As anticipated, in all 3 trajectories in which an extra water molecule was added to the binding pocket, tranylcypromine underwent a conformational change from its crystallographic pose to that of **i**, while there were still restraints on the protein atoms. Furthermore, all 3 trajectories maintained this tranylcypromine conformation for their duration. In 2 cases, the additional water molecule in the binding pocket maintained its position, while in a third, it simply exchanged positions with HOH415, providing further evidence that this position may be occupied by a bound water molecule. The continuation of the 3 previous trajectories without the extra water molecule in the binding pocket demonstrated the structural stability of conformations **i** and **ii**, for the 2 trajectories with tranylcypromine in conformation **i** at the end of the first nanosecond maintained this conformation for the subsequent 1.2 ns, and the third trajectory, which had tranylcypromine in conformation **ii** at 1 ns, maintained conformation **ii** for the subsequent 1.2 ns.

Based on the rapid conformational rearrangement of tranylcypromine in all the simulations, we suggest that the crystallographic binding pose be reconsidered. The crystallographic direct hydrogen bond between the tranylcypromine amino group and Gly219 is not stable in any of the simulations. Furthermore, the position occupied by this amino group in the crystallographic binding mode is occupied by a bound water molecule in 5 of the 6 nanosecond scale trajectories, and these 5 trajectories also share the same binding mode for tranylcypromine, conformation **i** in Figure 8. From the MD conformational data and the comparisons to the crystallographic binding mode of BPTI Lys15, we propose conformation **i**, with a water molecule located between tranylcypromine amino group and Gly219, the position currently occupied by tranylcypromine amino group in the X-ray structure, as an alternate model for fitting to the X-ray electron density. Placing an additional bound water molecule in the crystal structure is simpler than moving an already placed bound water and requiring subtle structural rearrangements to maintain hydrogen-bond networks, and the placement of an additional bound water in the binding pocket is not contraindicated based on comparison of the average energies for these two alternatives calculated from snapshots of the tight temperature control portions of the trajectories. Conformation **ii**, though less populated than conformation **i**, is also much more stable than the crystallographic binding pose and may also contribute to the experimentally observed electron density. This additional contribution could lead to difficulty in finding a single ligand conformation that accounts for the observed electron density.

The free energy of protein–ligand binding reflects a balance between protein–ligand and solvent–ligand interactions. Tranylcypromine's charge is more localized than benzamidine's, and this would lead to a more favorable solvent–ligand interaction energy for tranylcypromine. Additionally, the two distinct noncrystallographic binding poses that tranylcypromine is seen to assume are likely a reflection of its poorer structural–energetic complementarity with the binding pocket compared to benzamidine. Multiple binding modes for the low-affinity tranylcypromine may be a cause of ambiguous electron density with respect to positioning of the ligand, despite the 1.9-Å crystal resolution. The simulation results provide alternate, energetically preferred conformations to the crystallographic model tranylcypromine coordinates, and suggests reassignment of some electron density, currently ascribed to tranylcypromine's amino moiety, to a crystallographic water.

CONCLUSIONS

We have used MD simulations to study bovine trypsin complexed with two basic noncovalent small-molecule inhibitors, benzamidine and tranylcypromine. Benzamidine, which has hydrogen-bonding donor capacity identical to Arg side-chain, is found to preferentially sample two conformations having nonplanar internal geometries with equal probability. These conformations have torsion angles of ±25° in contrast to the nearly planar X-ray crystallographic benzamidine coordinates. The MD and X-ray data are nonetheless consistent, since the observed X-ray electron density is necessarily an average, and the thermal

average structure from the MD is planar. Tranylcypromine, which has hydrogen-bonding donor capacity identical to Lys side-chain, samples two conformations similar to each other. Both of these conformations' hydrogen-bonding patterns are the same as that of the BPTI Lys15 side-chain seen in a trypsin–BPTI cocrystal. This hydrogen-bonding pattern differs substantially from that in the trypsin–tranylcypromine X-ray structure coordinates: In the trypsin–tranylcypromine X-ray structure, the tranylcypromine amino group is placed in an area of high electron density directly adjacent to the backbone oxygen of trypsin Gly219, while in the trypsin–BPTI cocrystal structure, this position is occupied by a water molecule that bridges the trypsin Gly219 backbone oxygen and the BPTI Lys15 side-chain amino group. This bridging water is seen in MD of trypsin–tranylcypromine even though the simulations are started from the trypsin–tranylcypromine cocrystal coordinates, and occurs in simulations using three different molecular mechanics force fields.

ACKNOWLEDGMENTS

Our thanks to Professor David Case for providing Amber parameters for tranylcypromine.

REFERENCES

1. Broutin-L'Hermite I, Ries-Kautt M, Ducruix A. 1.7 Å X-ray structure of space-grown collagenase crystals. Acta Crystallogr D Biol Crystallogr 2000;56:376–378.
2. Lu D, Futterer K, Korolev S, Zheng X, Tan K, Waksman G, Sadler JE. Crystal structure of enteropeptidase light chain complexed with an analog of the trypsinogen activation peptide. J Mol Biol 1999;292:361–373.
3. Sommerhoff CP, Fang KC, Nadel JA, Caughey GH. Classical second messengers are not involved in proteinase-induced degranulation of airway gland cells. Am J Physiol 1996;271:L796–L803.
4. Fujinaga M, Chernaia MM, Halenbeck R, Koths K, James MN. The crystal structure of PR3, a neutrophil serine proteinase antigen of Wegener's granulomatosis antibodies. J Mol Biol 1996; 261:267–278.
5. Rotonda J, Garcia-Calvo M, Bull HG, Geissler WM, McKeever BM, Willoughby CA, Thornberry NA, Becker JW. The three-dimensional structure of human granzyme B compared to caspase-3, key mediators of cell death with cleavage specificity for aspartic acid in P1. Chem Biol 2001;8:357–368.
6. Ohbayashi H. Novel neutrophil elastase inhibitors as a treatment for neutrophil-predominant inflammatory lung diseases. IDrugs 2002;5:910–923.
7. Parfrey H, Mahadeva R, Lomas DA. Alpha(1)-antitrypsin deficiency, liver disease and emphysema. Int J Biochem Cell Biol 2003;35:1009–1014.
8. Budayova-Spano M, Lacroix M, Thielens NM, Arlaud GJ, Fontecilla-Camps JC, Gaboriaud C. The crystal structure of the zymogen catalytic domain of complement protease C1r reveals that a disruptive mechanical stress is required to trigger activation of the C1 complex. EMBO J 2002;21:231–239.
9. Gaboriaud C, Rossi V, Bally I, Arlaud GJ, Fontecilla-Camps JC. Crystal structure of the catalytic domain of human complement c1s: a serine protease with a handle. EMBO J 2000;19:1755–1765.
10. Jing H, Macon KJ, Moore D, DeLucas LJ, Volanakis JE, Narayana SV. Structural basis of profactor D activation: from a highly flexible zymogen to a novel self-inhibited serine protease, complement factor D. EMBO J 1999;18:804–814.
11. Jing H, Xu Y, Carson M, Moore D, Macon KJ, Volanakis JE, Narayana SV. New structural motifs on the chymotrypsin fold and their potential roles in complement factor B. EMBO J 2000;19:164–173.
12. Davidson CJ, Tuddenham EG, McVey JH. 450 million years of hemostasis. J Thromb Haemost 2003;1:1487–1494.
13. Berger P, Tunon-De-Lara JM, Savineau JP, Marthan R. Selected contribution: tryptase-induced PAR-2-mediated Ca(2+) signaling in human airway smooth muscle cells. J Appl Physiol 2001;91:995–1003.
14. Sato M, Yoshida S, Iida K, Tomozawa T, Kido H, Yamashita M. A novel influenza A virus activating enzyme from porcine lung: purification and characterization. Biol Chem 2003;384:219–227.
15. Kishi T, Kato M, Shimizu T, Kato K, Matsumoto K, Yoshida S, Shiosaka S, Hakoshima T. Crystal structure of neuropsin, a hippocampal protease involved in kindling epileptogenesis. J Biol Chem 1999;274:4220–4224.
16. Iwata A, Maruyama M, Akagi T, Hashikawa T, Kanazawa I, Tsuji S, Nukina N. Alpha-synuclein degradation by serine protease neurosin: implication for pathogenesis of synucleinopathies. Hum Mol Genet 2003;12:2625–2635.
17. Carvalho AL, Sanz L, Barettino D, Romero A, Calvete JJ, Romao MJ. Crystal structure of a prostate kallikrein isolated from stallion seminal plasma: a homologue of human PSA. J Mol Biol 2002;322:325–337.
18. Sidenius N, Blasi F. The urokinase plasminogen activator system in cancer: recent advances and implication for prognosis and therapy. Cancer Metastasis Rev 2003;22:205–222.
19. Blow DM. Structure and mechanism of chymotrypsin. Acc Chem Res 1976;9:145–152.
20. Watorek W. Azurocidin—inactive serine proteinase homolog acting as a multifunctional inflammatory mediator. Acta Biochim Pol 2003;50:743–752.
21. Bode W, Renatus M. Tissue-type plasminogen activator: variants and crystal/solution structures demarcate structural determinants of function. Curr Opin Struct Biol 1997;7:865–872.
22. Hollenberg MD. Proteinase-mediated signaling: proteinase-activated receptors (PARs) and much more. Life Sci 2003;74:237–246.
23. Branden C, Tooze J. Introduction to protein structure. New York: Garland; 1999.
24. Murzin AG, Brenner SE, Hubbard T, Chothia C. SCOP: a structural classification of proteins database for the investigation of sequences and structures. J Mol Biol 1995;247:536–540.
25. Bruestle M. Chemtool—Molekuele zeichnen mit dem Pinguin. Nachr Chem Tech Lab 2001;49:1310–1314.
26. Humphrey W, Dalke A, Schulten K. VMD: visual molecular dynamics. J Mol Graph 1996;14:33–38.
27. Stone JE. An efficient library for parallel ray tracing and animation. Intel Supercomputer Users Group Conference; 1995.
28. Marquart M, Walter J, Deisenhofer J, Bode W, Huber R. The geometry of the reactive site and of the peptide groups in trypsin, trypsinogen, and its complexes with inhibitors. Acta Crystallogr B 1983;39:480–490.
29. Kurinov IV, Harrison RW. Prediction of new serine proteinase inhibitors. Nat Struct Biol 1994;1:735–743.
30. Hartley BS, Kauffman DL. Corrections to the amino acid sequence of bovine chymotrypsinogen A. Biochem J 1966;101:229–231.
31. Mares-Guia M, Shaw E. Studies on the active center of trypsin: the binding of amidines and guanidines as models of the substrate side chain. J Biol Chem 1965;240:1579–1585.
32. Brooks BR, Bruccoleri RE, Olafson BD, States DJ, Swaminathan S, Karplus M. CHARMM—a program for macromolecular energy, minimization, and dynamics calculations. J Comput Chem 1983;4: 187–217.
33. MacKerell AD, Bashford D, Bellott M, Dunbrack RL, Evanseck JD, Field MJ, Fischer S, Gao J, Guo H, Ha S, Joseph-McCarthy D, Kuchnir L, Kuczera K, Lau FTK, Mattos C, Michnick S, Ngo T, Nguyen DT, Prodhom B, Reiher WE, Roux B, Schlenkrich M, Smith JC, Stote R, Straub J, Watanabe M, Wiorkiewicz-Kuczera J, Yin D, Karplus M. All-atom empirical potential for molecular modeling and dynamics studies of proteins. J Phys Chem B 1998;102:3586–3616.
34. Jorgensen WL, Chandrasekhar J, Madura JD, Impey RW, Klein ML. Comparison of simple potential functions for simulating liquid water. J Chem Phys 1983;79:926–935.
35. Roche O, Kiyama R, Brooks CL III. Ligand–protein database: linking protein–ligand complex structures to binding data. J Med Chem 2001;44:3592–3598.
36. Spartan. Irvine, CA: Wavefunction, Inc.
37. Press WH, Teukolsky SA, Vetterling WT, Flannery BP. Numerical recipes in C: the art of scientific computing. Cambridge, UK: Cambridge University Press; 1992.

38. Allen MP, Tildesley DJ. Computer simulation of liquids. Oxford, UK: Oxford University Press; 1987.
39. Ryckaert JP, Ciccotti G, Berendsen HJC. Numerical-integration of Cartesian equations of motion of a system with constraints—molecular dynamics of *N*-alkanes. J Comput Phys 1977;23:327–341.
40. Steinbach PJ, Brooks BR. New spherical-cutoff methods for long-range forces in macromolecular simulation. J Comput Chem 1994;15:667–683.
41. Levitt M, Lifson S. Refinement of protein conformations using a macromolecular energy minimization procedure. J Mol Biol 1969; 46:269–279.
42. Verlet L. Computer experiments on classical fluids: I. Thermodynamical properties of Lennard–Jones molecules. Phys Rev 1967; 159:98–103.
43. Feller SE, Zhang YH, Pastor RW, Brooks BR. Constant-pressure molecular-dynamics simulation—the Langevin piston method. J Chem Phys 1995;103:4613–4621.
44. Essex JW, Severance DL, Tirado-Rives J, Jorgensen JL. Monte Carlo simulations for proteins: binding affinities for trypsin–benzamidine complexes via free-energy pertrubations. J Phys Chem B 1997;101:9663–9669.
45. Bartunik HD, Summers LJ, Bartsch HH. Crystal structure of bovine beta-trypsin at 1.5 Å resolution in a crystal form with low molecular packing density: active site geometry, ion pairs and solvent structure. J Mol Biol 1989;210:813–828.
46. Bode W, Schwager P. The refined crystal structure of bovine beta-trypsin at 1.8 Å resolution: II. Crystallographic refinement, calcium binding site, benzamidine binding site and active site at pH 7.0. J Mol Biol 1975;98:693–717.
47. Huber R, Kukla D, Bode W, Schwager P, Bartels K, Deisenhofer J, Steigemann W. Structure of the complex formed by bovine trypsin and bovine pancreatic trypsin inhibitor: II. Crystallographic refinement at 1.9 Å resolution. J Mol Biol 1974;89:73–101.
48. Earnest T, Fauman E, Craik CS, Stroud R. 1.59 Å structure of trypsin at 120 K: comparison of low temperature and room temperature structures. Proteins 1991;10:171–187.
49. Brunger AT, Huber R, Karplus M. Trypsinogen–trypsin transition: a molecular dynamics study of induced conformational change in the activation domain. Biochemistry 1987;26:5153–5162.
50. Ota N, Stroupe C, Ferreira-da-Silva JM, Shah SA, Mares-Guia M, Brunger AT. Non-Boltzmann thermodynamic integration (NBTI) for macromolecular systems: relative free energy of binding of trypsin to benzamidine and benzylamine. Proteins 1999;37:641–653.
51. Luque I, Freire E. Structural stability of binding sites: consequences for binding affinity and allosteric effects. Proteins 2000; Suppl 4:63–71.
52. Rhodes G. Crystallography made crystal clear: a guide for users of macromolecular models. San Diego: Academic Press; 2000.
53. Bode W, Fehlhammer H, Huber R. Crystal structure of bovine trypsinogen at 1.8 Å resolution: I. Data collection, application of patterson search techniques and preliminary structural interpretation. J Mol Biol 1976;106:325–335.
54. Fehlhammer H, Bode W, Huber R. Crystal structure of bovine trypsinogen at 1.8 Å resolution: II. Crystallographic refinement, refined crystal structure and comparison with bovine trypsin. J Mol Biol 1977;111:415–438.
55. Kossiakoff AA, Chambers JL, Kay LM, Stroud RM. Structure of bovine trypsinogen at 1.9 Å resolution. Biochemistry 1977;16:654–664.
56. Huber R, Bode W. Structural basis of the activation and action of trypsin. Acc Chem Res 1978;11:114–122.
57. Walter J, Steigemann W, Singh TP, Bartunik H, Bode W, Huber R. On the disordered activation domain in trypsinogen: chemical labelling and low-temperature crystallography. Acta Crystallogr B 1982;38:1462–1472.
58. Bode W, Walter J, Huber R, Wenzel HR, Tschesche H. The refined 2.2 Å (0.22 nm) X-ray crystal structure of the ternary complex formed by bovine trypsinogen, valine–valine and the Arg15 analogue of bovine pancreatic trypsin inhibitor. Eur J Biochem 1984;144:185–190.
59. Grzesiak A, Helland R, Smalas AO, Krowarsch D, Dadlez M, Otlewski J. Substitutions at the P(1) position in BPTI strongly affect the association energy with serine proteinases. J Mol Biol 2000;301:205–217.
60. Zhu Y, Huang Q, Qian M, Jia Y, Tang Y. Crystal structure of the complex formed between bovine beta-trypsin and MCTI-A, a trypsin inhibitor of squash family, at 1.8-Å resolution. J Protein Chem 1999;18:505–509.
61. Cornell WD, Cieplak P, Bayly CI, Gould IR, Merz Jr. KM, Ferguson DM, Spellmeyer DC, Fox T, Caldwell JW, Kollman PA. A second generation force field for the simulation of proteins, nucleic acids, and organic molecules. J Am Chem Soc 1995;117: 5179–5197.
62. Kaminski GA, Friesner RA, Tirado-Rives J, Jorgensen WL. Evaluation and reparametrization of the OPLS-AA force field for proteins via comparison with accurate quantum chemical calculations on peptides. J Phys Chem B 2001;105:6474–6487.
63. Jorgensen WL, Maxwell DS, Tirado-Rives J. Development and testing of the OPLS all-atom force field on conformational energetics and properties of organic liquids. J Am Chem Soc 1996;118: 11225–11236.
64. Wang J, Wolf RM, Caldwell JW, Kollman PA, Case DA. Development and testing of a general AMBER force field. J Comput Chem 2004;25:1157–1174.
65. Price DJ, Brooks CL III. Modern protein force fields behave comparably in molecular dynamics simulations. J Comput Chem 2002;23:1045–1057.